STEPHY Publishers

Current Investigations in Clinical and Medical Research

Case Report

ISSN: 2770-6133

Coronal Plane Deformity Correction in Diaphyseal Tibial Malunion Following Intramedullary Nailing: A DIY Workflow Using Patient-Specific 3D-Printed Resin Osteotomy Guides

Sergio Pérez Ortiz,* Jesús García Álvarez, Rebeca Sánchez Mateo, Carlos Sánchez Monzó, Carlos Guillermo Puig Abbs

Hospital Intermutual de Levante, San Antonio de Benagéber, Valencia, Spain

Abstract

Background: Diaphyseal tibial malunion with coronal plane deformity following intramedullary nailing is a challenging reconstructive problem. Corrective osteotomy at the deformity apex requires precise intraoperative reproduction of the planned angular correction, which is difficult to achieve by conventional freehand techniques in a revision setting with hypertrophic callus. Patient-specific 3D-printed osteotomy guides, designed and fabricated entirely in-house, represent an accessible and low-cost strategy to transfer the preoperative plan directly to the surgical field with geometric accuracy.

Case Presentation: A 63-year-old male construction worker presented with symptomatic varus malalignment of the left tibia two years after intramedullary nailing of a proximal diaphyseal fracture (AO/OTA 41-A2). CT and full-length standing radiographs confirmed an 11.23° coronal plane varus deformity with hypertrophic callus and a 1.5cm limb length discrepancy. Following implant removal, two patient-specific osteotomy guides were designed in-house from CT-based 3D reconstruction and fabricated in photopolymer resin using a desktop LCD printer, then sterilised by low-temperature hydrogen peroxide plasma. Intraoperatively, the guides were applied to the lateral tibial cortex and secured with Kirschner wires, defining both osteotomy planes and the medial cortical hinge with the correction angle encoded in the guide geometry. A lateral closing-wedge osteotomy was performed and fixed with a pre-contoured 4.5mm locking compression plate, with concomitant fibular osteotomy through a separate incision.

Results: Intraoperative fluoroscopy and immediate postoperative radiographs confirmed complete correction of the varus deformity. CT at seven months demonstrated advanced consolidation at the osteotomy site. The patient returned to full occupational activity at six months. SF-36 improved from 68 to 96 at three-year follow-up.

Conclusion: In-house patient-specific resin osteotomy guides enable precise angular correction in diaphyseal tibial malunion, with satisfactory clinical and functional outcomes at mid-term follow-up.

Keywords: Tibial malunion, Corrective osteotomy, Patient specific instrumentation, 3D Printing, Intramedullary nail, Varus deformity, Coronal plane, DIY surgical guides

Abbreviations: PIN: Posterior Interosseous Nerve; NA: Neuralgic Amyotrophy; AIN: Anterior Interosseous Nerve; EMG: Electromyography; MRC: Medical Research Council; ORIF: Open Reduction and Internal Fixation

Introduction

Tibial shaft fractures are among the most frequent long bone injuries managed by orthopaedic surgeons worldwide. Intramedullary nailing remains the standard of care for displaced diaphyseal tibial fractures, providing reliable stability and acceptable rates of union. Nevertheless, malunion-defined as consolidation in a clinically unacceptable position-occurs in up to 20% of tibially nailed fractures, with rates notably higher for fractures of the proximal and distal thirds of the diaphysis.[1,2] The resulting deformities may involve the coronal, sagittal, or

*Corresponding author: Sergio Pérez Ortiz, Hospital Intermutual de Levante, Km 11,7 CV-35, 46184 San Antonio de Benagéber, Valencia, Spain

Quick Response Code:

Received: 11 March, 2026 **Published:** 23 March, 2026

Citation: Pérez Ortiz S, García Álvarez J, Sánchez Mateo R, Sánchez Monzó C, Puig Abbs CG. Coronal Plane Deformity Correction in Diaphyseal Tibial Malunion Following Intramedullary Nailing: A DIY Workflow Using Patient-Specific 3D-Printed Resin Osteotomy Guides: Case Report. Curr Inv Cln Med Res. 2026;4(1):1–8. DOI:10.53902/CICMR.2026.04.000529

axial planes in isolation or in combination, and are associated with progressive joint overload, gait disturbance, and secondary osteoarthritis of the knee and ankle.[3,4]

Coronal plane varus deformity of the tibial diaphysis is particularly consequential from a biomechanical standpoint. Altered mechanical axis alignment redistributes medial compartment loading at the knee and modifies tibiotalar contact forces, with demonstrated correlation between tibial angular deformity and degenerative joint disease.[3,5] Symptomatic malunion in an active, working-age patient therefore constitutes a clear surgical indication, provided the benefits of correction justify the inherent risks of revision bone surgery.

Corrective osteotomy has been the cornerstone of treatment for diaphyseal tibial malunion for decades. Multiple techniques have been described-closing-wedge, opening-wedge, oblique single-cut, dome, and clamshell osteotomies-each with distinct biomechanical properties, technical demands, and fixation requirements.[6-8] The fundamental surgical challenge is the accurate transfer of the preoperative angular correction plan to the intraoperative field. Conventional methods relying on fluoroscopic K-wire triangulation and freehand osteotomy carry inherent imprecision, particularly in the context of hypertrophic callus and previously instrumented tissue, where anatomical landmarks are distorted.

The advent of computer-assisted surgical planning and additive manufacturing has introduced a new paradigm for osteotomy precision. Patient-specific instruments designed from segmented CT data encode the planned osteotomy plane within a guide that physically fits the patient's bone surface, eliminating intraoperative geometric estimation. The clinical evidence supporting PSI-assisted corrective osteotomy has grown substantially in the past decade, with reported improvements in correction accuracy, reductions in operative time, and decreased fluoroscopic exposure compared with conventional techniques.[9-11] Critically, the progressive democratisation of 3D printing technology-reflected in the availability of affordable desktop resin printers and open-source segmentation software has made it feasible for motivated surgical teams to implement in-house PSI workflows at a fraction of the cost of commercial solutions.[12,13]

We present a case of symptomatic proximal diaphyseal tibial varus malunion following intramedullary nailing, managed with a fully surgeon-directed DIY workflow for the design and fabrication of patient-specific resin osteotomy guides, and discuss the technical considerations, clinical outcome, and broader implications of this approach.

Case Report

Clinical presentation

A 63 -year-old male construction worker was referred for assessment of a left tibial malunion. He had sustained a proximal diaphyseal tibial fracture classified as AO/OTA 41-A2, treated with an anterograde T2 intramedullary nail at a different institution. Despite radiographic consolidation, the patient had a varus deformity of the left lower limb due to malunion, clearly visible in the standing position on frontal inspection. He reported intermittent bilateral peripatellar discomfort, without evidence of instability or limitation of knee range of motion. There was no history of infection and wound healing had been uneventful. His medical history was unremarkable except for mild hypertension and a prior appendicectomy; no chronic medications were used.

Figure 1 Clinical photograph, anterior view, demonstrating visible varus malalignment of the left lower limb in the standing position. The coronal plane deformity is evident on frontal inspection, with the left leg showing a clear bowing compared to the contralateral limb.

Physical examination confirmed complete healing of prior incisions, a full arc of knee flexion-extension, and no varus-valgus instability. In standing alignment, varus malalignment of the left limb was clinically evident. Full-length lower limb radiographs demonstrated a left limb total length of 91.2cm compared with 90.4cm on the right, yielding a discrepancy of approximately 1.5cm. CT of the left tibia confirmed complete consolidation of the proximal diaphyseal fracture with bilateral hypertrophic callus formation and a coronal plane varus deformity measuring 11.23°. No clinically dominant rotational or sagittal plane component was identified.

Figure 2 Anteroposterior radiograph of the left tibia showing the intramedullary nail in situ and the coronal plane varus deformity at the proximal diaphysis, with hypertrophic callus at the fracture site.

Given the symptomatic nature of the deformity, the patient's occupation, and his age, surgical correction was indicated. A two-stage strategy was adopted: first, removal of the intramedullary device to allow CT-based 3D bone reconstruction without metallic artefact; second, corrective osteotomy of the tibia one month after.

Three dimensional planning and guide design

Three-dimensional reconstruction of the tibia was performed from CT DICOM data using 3D Slicer (version 4.11.2, open-source).

Bone segmentation was performed using a semi-automated threshold-based approach with manual correction of ambiguous regions, yielding a patient-specific surface mesh of the left tibia. Deformity analysis confirmed the 11.23° varus angulation in the coronal plane, with the deformity apex located at the proximal diaphysis corresponding to the callus zone.

Figure 3 Three-dimensional virtual model of the left tibia obtained from CT segmentation, displaying the hypertrophic callus at the fracture site and the angular deformity in the coronal plane.

The correction plan consisted of a laterally-based closing-wedge osteotomy at the CORA (centre of rotation of angulation), with resection of a bone wedge whose apex was at the medial cortex. A concomitant simple oblique fibular osteotomy was planned through a separate approach.

Guide design was performed in Meshmixer (v. 3.5.474). Two patient-specific instruments were designed to fit the lateral cortical surface of the proximal tibia, exploiting the irregular topography of the hypertrophic callus as a registration feature to ensure a unique and reproducible seating position. Each guide incorporated cylindrical tunnels for the passage of 1.5 mm Kirschner wires for guide stabilization and 2.0mm Kirschner wires, oriented to define the proximal and distal osteotomy planes with the 11.23° correction angle encoded in the relative orientation of the tunnel pairs, for the osteotomy.

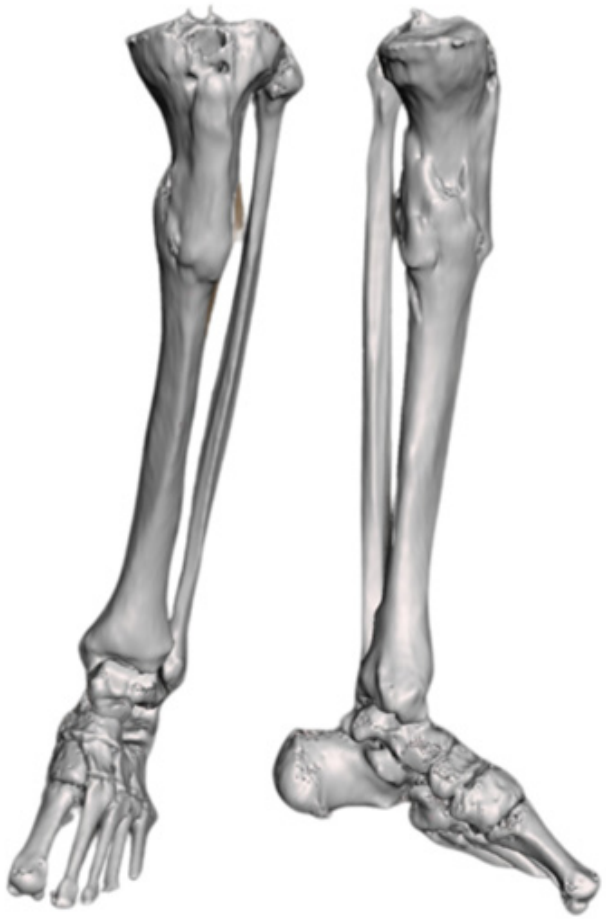

Figure 4 Computer-aided design of the two patient-specific osteotomy guides, showing their surface geometry adapted to the lateral tibial cortex and the cylindrical tunnels for Kirschner wire guidance. Virtual simulation of guide seating on the 3D tibial model demonstrates the planned fit and orientation of the osteotomy planes.

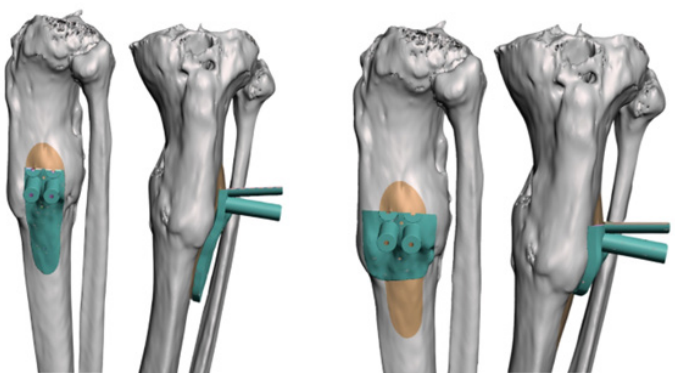

Figure 5 Virtual simulation with the guides in position and the Kirschner wires inserted through the guide tunnels, projecting the proximal and distal osteotomy planes and delineating the bone wedge to be respected.

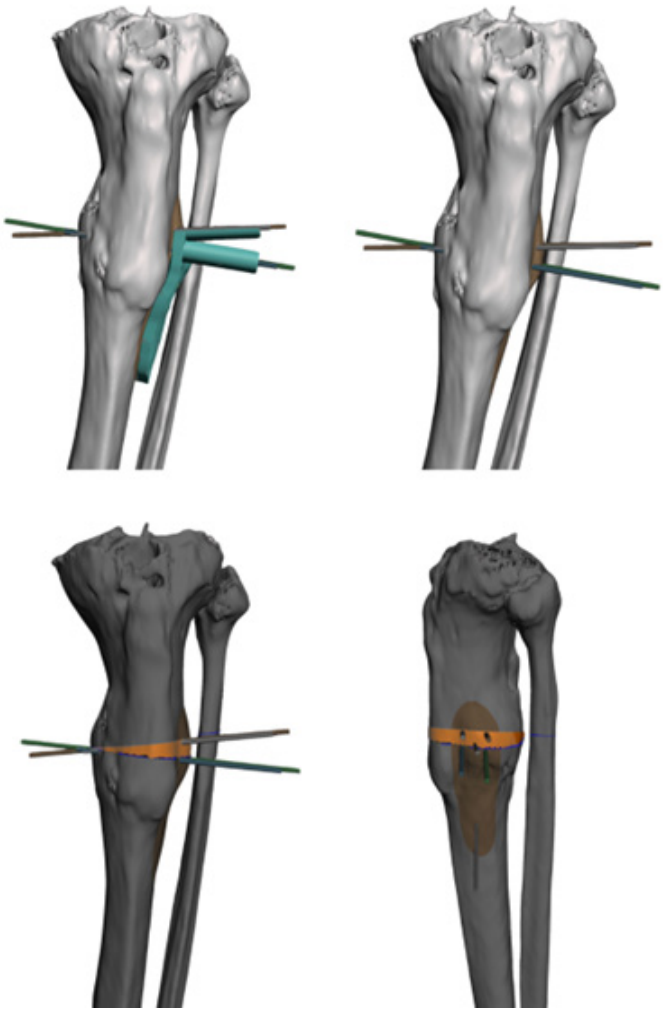

Figure 6 Virtual simulation of the osteotomy: the bone wedge has been subtracted from the 3D model, illustrating the planned correction of the varus deformity and the restored coronal alignment following wedge closure.

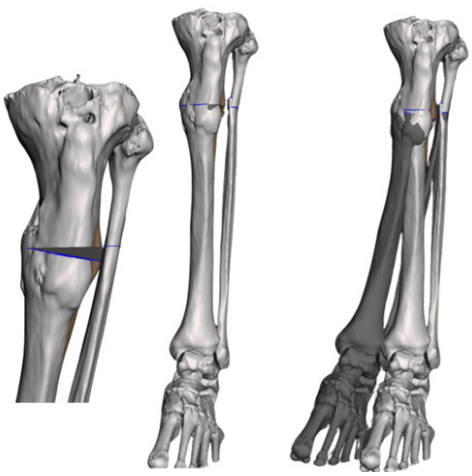

The guides were fabricated using an Anycubic LCD resin desktop printer (water-washable photopolymer resin) with a layer thickness of 0.05 mm. post-processing included water cleaning and UV post-curing. Physical fit of the guides was verified on a 3D-printed tibial model prior to sterilisation, and minor surface adjustments were made to optimise seating. Sterilisation was performed by low-temperature hydrogen peroxide plasma for intraoperative use.

Surgical technique

Surgery was performed under spinal anaesthesia with tourniquet control. A lateral approach to the proximal tibial diaphysis was made, with fascial opening and blunt muscle dissection. Subperiosteal dissection was carried out in the zone of the hypertrophic callus, exposing the lateral cortex. The narrow patient-specific guide was applied to the lateral tibial surface, and its seating was verified visually by confirming full cortical contact along the guide footprint. The guide was secured with 1.5mm K-wires through the stabilisation tunnels, and fluoroscopic confirmation of guide position was obtained in both anteroposterior and lateral projections.

Figure 7 Intraoperative photograph showing the patient-specific resin guides checking proper insertion of the K-wires, the guides applied to the lateral tibial cortex, with Kirschner wires passed through the guide tunnels defining the osteotomy planes.The guide surface conforms to the tibial cortex and callus topography.

The 2.0mm directional K-wires were then drilled through the guide tunnels, projecting the proximal and distal osteotomy planes across the tibial cross-section. The guide was removed after wire placement, leaving the directional K-wires in situ.

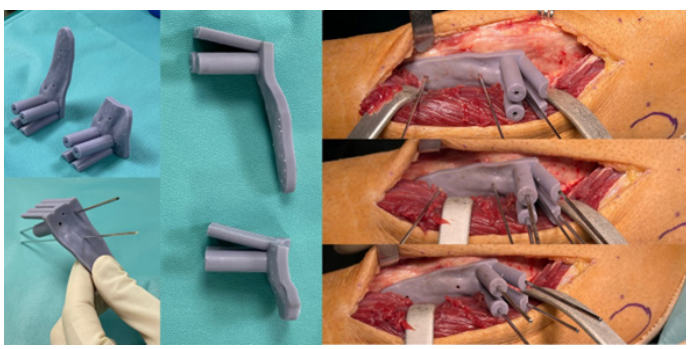

Figure 8 Intraoperative fluoroscopic image demonstrating the Kirschner wires in the planned osteotomy orientations, confirming the angular disposition corresponding to the preoperative correction plan.

The osteotomy was performed with an oscillating saw along the K-wire planes and completed with an osteotome to preserve the medial cortical hinge. The laterally-based bone wedge was extracted en bloc.

Figure 9 Intraoperative photograph after completion of the osteotomy, showing the open wedge defect in the lateral tibial cortex before wedge closure and a close-up view of the resected bone wedge alongside the osteotomy site. The wedge geometry corresponds to the preoperative plan, confirming adequate guide-directed bone resection.

The osteotomy was closed by manual compression, confirming absence of rotational change during closure. Intraoperative fluoroscopy confirmed satisfactory coronal alignment and wedge closure. Fixation was achieved with a 4.5-mm eight-hole Locking Compression Plate (LCP; DePuy Synthes, Oberdorf, Switzerland) applied to the lateral tibial cortex and secured provisionally with K-wires before definitive fixation with cortical and locking screws.

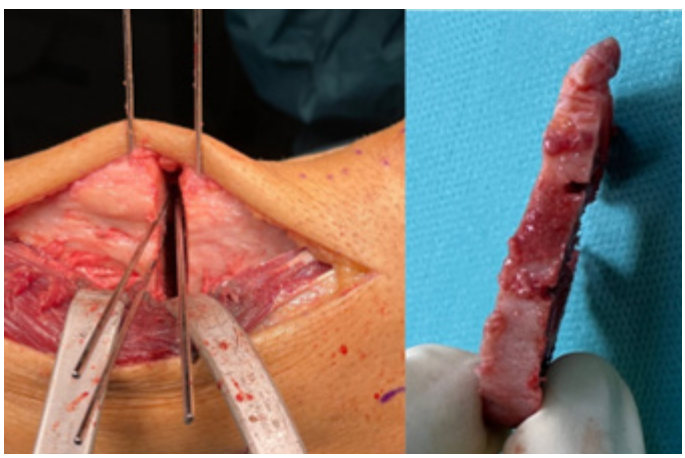

Figure 10 Intraoperative photograph of the closed osteotomy secured with the pre-contoured lateral locking compression plate, with provisional K-wires in place prior to definitive screw fixation.

A separate limited approach was used to perform a simple oblique osteotomy of the fibular diaphysis. Wound closure was performed by planes over a subfascial Redon drain. Tourniquet was deflated and distal circulation confirmed.

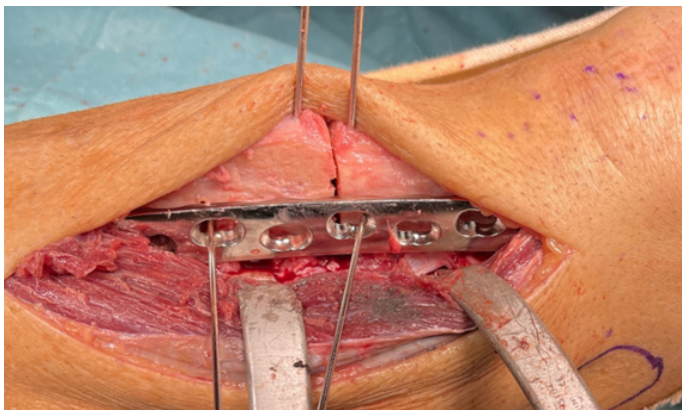

Results

Immediate postoperative anteroposterior and lateral radiographs confirmed satisfactory implant positioning and complete correction of the preoperative varus deformity, with restoration of the mechanical axis in the coronal plane.

Figure 11 Postoperative standing anteroposterior radiograph demonstrating correction of the coronal plane varus deformity, with the locking compression plate in satisfactory position and restored mechanical axis alignment.

Wound healing was uncomplicated at the two-week review. Sutures were removed without incident and no signs of superficial or deep infection were present. At six weeks, the patient was pain-free and radiographically showed early periosteal callus formation at the osteotomy site. CT performed at seven months confirmed advanced consolidation with bridging hypertrophic callus at the tibial osteotomy site, with a persistent but thinning fracture line, and consolidation progressing at the fibular osteotomy. No implant failure, periimplant fracture, or loss of correction was observed.

The patient was permitted partial weight-bearing at six weeks and progressed to full weight-bearing at twelve weeks. He returned to his full-time construction work at six months postoperatively. At the three-year follow-up, no pain was reported, limb alignment was clinically and radiologically maintained, and there were no functional limitations.

Figure 12 Clinical photographs showing frontal view comparison of the lower limbs before and after surgery, demonstrating the pre-existing varus deformity of the left limb and its correction at follow-up, with restored symmetrical alignment.

Figure 13 Full-length standing telemetric radiograph at follow-up confirming restoration of mechanical axis alignment of the left lower limb and absence of limb length discrepancy.

SF-36 score improved from 68 points preoperatively to 96 points at three-year follow-up, reflecting a clinically meaningful improvement in health-related quality of life across physical, functional, and social domains.

Discussion

The management of diaphyseal tibial malunion following intramedullary nailing presents specific technical challenges that distinguish it from primary fracture surgery. The malunited bone is hypertrophic, avascular in its callus core, and surrounded by scarred soft tissue planes that limit intraoperative visual and tactile feedback. In this context, the preoperative definition of the osteotomy plane and correction angle cannot rely solely on intraoperative fluoroscopic estimation without accepting a meaningful risk of residual deformity.

The literature on corrective osteotomy for diaphyseal tibial malunion spans a broad range of techniques. Classical series by Sanders [14] and Sangeorzan[15] described oblique and mathematically-directed single-cut osteotomies for uniplanar and biplanar deformities, achieving satisfactory correction with conventional radiographic planning. Wu[16] reported 37 cases of tibial shaft malunion treated with reamed intramedullary re-nailing, achieving residual angulation under 10° in all patients. The Taylor Spatial Frame has demonstrated millimetric precision in both angular and translational correction across multiple planes, though at the cost of significant patient burden and pin-site morbidity.[17] The clamshell osteotomy described by Russell[7] offers the versatility of combined angular, rotational, and translational correction using the nail as a reduction template, and is particularly applicable to diaphyseal malunions where the medullary canal remains accessible. In the present case, the prior nail had already been removed by the time definitive correction was planned, and the hypertrophic diaphyseal callus made intramedullary re-instrumentation technically hazardous; a lateral plating strategy was therefore preferred. The closing-wedge osteotomy was selected over an opening-wedge

configuration because it avoids the creation of a bone defect in an already compromised diaphyseal zone, and the presence of hypertrophic callus provided an adequate biological environment for healing under compression.

The central technical innovation in this case is the design and fabrication of patient-specific osteotomy guides entirely within the hospital setting, without recourse to commercial planning services. The concept of in-house PSI for corrective osteotomy has been described for the tibia and femur, with the seminal work of Pérez-Mañanes[13] demonstrating that self-manufactured 3D-printed cutting guides for high tibial osteotomy are feasible and accurate within a hospital environment. D'Amelio[9] have reviewed the role of 3D-printed PSI in corrective osteotomies of the lower extremity, emphasising that the technique allows preoperative planning to be reproduced at submillimetre precision when guide seating is verified and optimised. Mao[18] demonstrated in a prospective comparative study of medial opening-wedge high tibial osteotomy that PSI-guided correction achieved significantly lower angular errors than conventional freehand techniques (mFTA error 0.2° ± 0.6° versus 1.2° ± 1.4°, p = 0.004), with shorter operative time and less fluoroscopic exposure. These benefits are likely to be amplified in diaphyseal malunion surgery, where the absence of recognisable articular landmarks makes freehand angular estimation less reliable than in periarticular osteotomies. The computer-assisted single-cut oblique rotation osteotomy described by Dobbe[19] for complex tibial multiplanar malunion illustrates how 3D-guided planning can resolve deformities that would be geometrically intractable by conventional means; the approach in our case was comparatively straightforward in that only the coronal plane required correction, allowing a standard closing-wedge design guided by two dedicated K-wire tunnels in each guide.

An important consideration in the use of resin-based in-house guides is their dimensional stability and microbiological safety after sterilisation. The present case employed low-temperature hydrogen peroxide plasma sterilisation, which avoids the thermal stresses of steam autoclaving and has been shown to maintain dimensional accuracy in resin-printed guides. Sharma[20] demonstrated that steam sterilisation of biocompatible resin guides used for surgical navigation produces minimal dimensional change within clinically acceptable tolerances, though material-dependent variability exists. The more recent work of Kronenberger[21] on photopolymer resins for cardiac surgical guides highlights that sterilisation can modify mechanical and thermal properties, particularly when high-temperature steam is applied to heat-sensitive polymers. The Anycubic water-washable resin used in this case is not a certified Class IIa medical device resin in the strict regulatory sense; this limitation is shared by the majority of in-house PSI workflows reported in the literature and represents an area requiring further regulatory clarification as point-of-care manufacturing becomes more prevalent. From a practical standpoint, the guide performed as designed: intraoperative fit was adequate, K-wire placement was achieved through the planned tunnels without difficulty, and fluoroscopic confirmation showed a satisfactory osteotomy orientation before bone resection.

The patient reported no symptoms attributable to the corrected alignment and was fully functional at work. Nevertheless, sometimes overcorrection can be present. In closing-wedge osteotomy, the closing force applied to the bone wedge is the final determinant of the achieved angle, and intraoperative fluoroscopic estimation of the correction angle carries a margin of error that is difficult to eliminate without geometric feedback. A dedicated closing-wedge spacer printed at the planned resection angle-as described by Van Genechten[22] for high tibial osteotomy-might provide additional angular control at the moment of plate fixation, and represents a refinement worth incorporating into future iterations of this DIY workflow.

Several limitations of this case report must be acknowledged. Single-case reports do not provide the level of evidence required to draw generalisable conclusions regarding the superiority of PSI-guided DIY osteotomy over conventional techniques in diaphyseal tibial malunion. The absence of a contralateral CT used as a reference anatomical template which is standard practice in PSI planning workflows for complex deformities[9,10] means that the correction target was based on deformity-angle analysis alone rather than a mirrored reconstruction of the unaffected tibia. In a pure coronal plane deformity of this degree, this approach is acceptable, but for multiplanar malunions it would introduce significant error. Finally, the SF-36 instrument, while widely used, provides a global health status measure rather than a condition-specific functional score; future cases of this type would benefit from the addition of a validated lower-limb-specific outcome measure such as the LEFS or PROMIS Physical Function.[23-25]

Conclusion

This case demonstrates that a complete, surgeon-directed DIY workflow from CT segmentation and deformity analysis through 3D-printed guide fabrication and intraoperative use is feasible and clinically effective for the correction of coronal plane deformity in diaphyseal tibial malunion following intramedullary nailing. The approach achieved full correction of an 11° varus deformity with satisfactory functional outcome and return to heavy manual work at six months. The growing availability of open-source segmentation tools and low-cost resin printers positions in-house PSI manufacturing as a realistic option for surgical teams willing to invest in the learning curve. Further multicentre studies comparing DIY PSI-guided diaphyseal osteotomy with conventional techniques are needed to establish its accuracy, safety profile, and cost-effectiveness in a larger patient population.

Acknowledgments

None.

Funding

This Case Report received no external funding.

Conflicts of Interest

The authors declare no conflicts of interest relevant to this publication.

References

1. Kocadal O, Erçin E, Kose O, et al. Malunion of the tibia: a systematic review. *Medicina (Kaunas).* 2022;58(3):389.
2. Johnson EE. Multiplane correctional osteotomy of the tibia for diaphyseal malunion. *Clin Orthop Relat Res.* 1987;215:223-232.
3. Weinberg DS, Park PJ, Liu RW. Association between tibial malunion deformity parameters and degenerative hip and knee disease. *J Orthop Trauma*. 2016;30(9):510-515.
4. Milner SA, Davis TR, Muir KR, et al. Long-term outcome after tibial shaft fracture: is malunion important? *J Bone Joint Surg Am*. 2002;84(6):971-980.
5. Tarr RR, Resnick CT, Wagner KS, et al. Changes in tibiotalar joint contact areas following experimentally induced tibial angular deformities. *Clin Orthop Relat Res*. 1985;199:72-80.
6. Paley D, Chaudray M, Pirone AM, et al. Treatment of malunions and mal-nonunions of the femur and tibia by detailed preoperative planning and the Ilizarov techniques. *Orthop Clin North Am.* 1990;21(4):667-691.
7. Purcell KF, Russell GV, Graves ML. The clamshell osteotomy for diaphyseal malunion in deformity correction and fracture surgery. *Medicina (Kaunas).* 2021;57(9):951.
8. Sanders R, Anglen JO, Mark JB. Oblique osteotomy for the correction of tibial malunion. *J Bone Joint Surg Am*. 1995;77(2):240-246.
9. D'Amelio A, Van Lieshout EMM, Wakker AM, et al. 3D-printed patient-specific instruments for corrective osteotomies of the lower extremity. *Injury.* 2022;53Suppl 3:S53-S58.
10. Dobbe JGG, du Pre KJ, Blankevoort L, et al. Computer-assisted oblique single-cut rotation osteotomy to reduce a multidirectional tibia deformity: case report. *Strategies Trauma Limb Reconstr*. 2017;12(1):49-55.
11. Long J, Linyun Tan, Xiaoyan Liu. Applications and clinical outcomes of 3D printing technology in orthopedic trauma surgery. *Front Med (Lausanne).* 2025;12:1560909.
12. Perez Mananes R, Burro JA, Manaute JR, et al. 3D surgical printing cutting guides for open-wedge high tibial osteotomy: do it yourself. *J Knee Surg*. 2016;29(8):690-695.
13. Mao Y, Xiong Y, Li Q, et al. 3D-printed patient-specific instrumentation technique vs. conventional technique in medial open-wedge high tibial osteotomy: a prospective comparative study. *Biomed Res Int.* 2020;2020:1923172.
14. Sangeorzan BJ, Hansen ST, Judd RP. Mathematically directed single-cut osteotomy for correction of tibial malunion. *J Orthop Trauma*. 1989;3(4):267-275.
15. Mast JW, Teitge RA, Gowda M. Preoperative planning for the treatment of nonunions and the correction of malunions of the long bones. *Orthop Clin North Am*. 1990;21(4):693-714.
16. Wu CC, Chen WJ, Shih CH. Tibial shaft malunion treated with reamed intramedullary nailing: a revised technique. *Arch Orthop Trauma Surg*. 2000;120(3-4):152-156.
17. Feldman DS, Shin SS, Madan S, et al. Correction of tibial malunion and nonunion with six-axis analysis deformity correction using the Taylor Spatial Frame. *J Orthop Trauma*. 2003;17(8):549-554.
18. Furnstahl P, Vlachopoulos L, Schweizer A, et al. Complex osteotomies of tibial plateau malunions using computer-assisted planning and patient-specific surgical guides. *J Orthop Trauma*. 2015;29(8):e270-e276.
19. Munier M, Donnez M, Ollivier M, et al. Can three-dimensional patient-specific cutting guides be used to achieve optimal correction for high tibial osteotomy? Pilot study. *Orthop Traumatol Surg Res*. 2017;103(2):245-250.
20. Sharma N, Cao S, Msallem B, et al. Effects of steam sterilization on 3D printed biocompatible resin materials for surgical guides: an accuracy assessment study. *J Clin Med*. 2020;9(5):1506.
21. Kronenberger R, Kazma R, Amirabadi A, et al. Impact of disinfection and sterilization on 3D-printing resin performance for surgical guides in cardiac ablation surgery. *Bioengineering (Basel).* 2025;12(9):924.
22. Yang JCS, Chen CF, Luo CA, et al. Clinical experience using a 3D-printed patient-specific instrument for medial opening-wedge high tibial osteotomy. *Biomed Res Int*. 2018;2018:9246529.
23. Ali M, Alalawi A, et al. Association of fracture location and pattern with nonunion or malunion in tibia fractures managed with intramedullary nailing. *Cureus*. 2023;15(4):e37623.
24. Graehl PM, Hersh MR, Heckman JD. Supramalleolar osteotomy for the treatment of symptomatic tibial malunion. *J Orthop Trauma*. 1987;1(4):281-292.
25. Hu K, Zhao L, Liu Z, et al. The efficacy of 3D printing model in the intraarticular osteotomy in the treatment of tibial plateau fractures. *Orthop Surg*. 2023;15(1):84-93.